CrossMark

Electromagnetic energy transport by tearing fluctuations in a self-organized reversed-field pinch plasma

Derek J. Thuecks [1],† **and Karsten J. McCollam** [2]

[1]Department of Physics, Washington College, 300 Washington Avenue, Chestertown, MD 21620, USA

[2]Department of Physics, University of Wisconsin–Madison, 1150 University Avenue, Madison, WI 53706, USA

Fluctuation measurements reveal the outward electromagnetic energy flux needed to drive the dynamo electromotive force supporting magnetic self-organization in a reversed-field pinch plasma. The radial Poynting flux due to tearing mode fluctuations is measured with an insertable probe during magnetic relaxation. This flux corresponds to transient power levels much larger than the input power and comparable to the global equilibrium magnetic energy transient loss rate. The probe measurements of this flux are roughly as predicted by a simple Poynting's theorem model upon substitution of equilibrium measurement data.

Key words: plasma dynamics, plasma nonlinear phenomena, plasma instabilities

1. Introduction

Magnetic self-organization processes determine the signature equilibrium configuration of reversed-field pinch (RFP) plasmas (Marrelli *et al.* 2021) driven by steady induction. In these RFP plasmas, the toroidal magnetic field is peaked in the core, decreases monotonically with minor radius and reverses direction near the plasma edge. While the applied loop voltage drive tends to peak the equilibrium radial profile of field-normalized parallel current density, magnetic relaxation (Taylor 1974) due to nonlinearly interacting tearing modes (Ho & Craddock 1991) tends to flatten it, an interplay that can take the form of a sawtooth cycle. During a discrete, spontaneous relaxation event or sawtooth crash, magnetic tearing rapidly becomes nonlinear and multimode. Core toroidal current density is suppressed, as poloidal current in the edge is enhanced by a tearing fluctuation-induced 'dynamo' electromotive force (EMF) $\langle \boldsymbol{v}_1 \times \boldsymbol{B}_1 \rangle_\parallel$ parallel to the local equilibrium magnetic field, where $\boldsymbol{v}_1$ and $\boldsymbol{B}_1$ represent velocity and magnetic field fluctuations and brackets indicate flux-surface averaging (Ortolani & Schnack 1993). This relaxation event increases the equilibrium toroidal magnetic flux, and the cycle continues.

Much is known about the RFP magnetic self-organization process. In particular, excitation of core-resonant tearing modes, nonlinear interactions between these modes with modes resonant at the reversal surface, and the resulting energization of the dynamo

† Email address for correspondence: dthuecks2@washcoll.edu

EMF have all been well studied in magnetohydrodynamics (MHD) computation (Nebel, Caramana & Schnack 1989; Ho & Craddock 1991; Ortolani & Schnack 1993; Sauppe & Sovinec 2017). Detailed measurements of the dynamo EMF have been made in experiment (Ji *et al.* 1994; den Hartog *et al.* 1999; Fontana *et al.* 2000; Kuritsyn *et al.* 2009). One aspect of the process that has not received much attention is the role of magnetic tearing fluctuations in transporting electromagnetic energy from the core, where magnetic energy is released during relaxation, to the edge, where it becomes available to power dynamo EMF current drive.

To date, much of the work that has been done to understand energy transport in RFP plasmas has focused on thermal energy transport. In the RFP, radial magnetic field fluctuations due to tearing modes produce a stochastic magnetic field in the core resulting in particle and thermal energy transport from the core to the edge plasma due to field-parallel streaming (Fiksel *et al.* 1996; Serianni *et al.* 2001; Biewer *et al.* 2003). While this stochastic field effect accounts for most of the thermal transport through much of the plasma (Biewer *et al.* 2003), it only accounts for $<30\%$ of the power lost from the extreme edge plasma (Fiksel *et al.* 1996). Previous studies have shown that electrostatic turbulence is largely responsible for particle losses but can only explain $\sim10\%$ of the measured thermal energy transport in the edge (Rempel *et al.* 1991, 1992; Brunsell *et al.* 1994). The mechanisms responsible for thermal energy losses at the extreme edge and their relative weights remain incompletely specified.

In this work, electromagnetic energy transport, which is distinct from thermal energy transport, is examined. The tearing fluctuation-induced Poynting flux is written as $S_f = \mu_0^{-1} \int \langle \boldsymbol{E}_1 \times \boldsymbol{B}_1 \rangle \cdot \mathrm{d}\boldsymbol{A}$, where coherent fluctuations in electric and magnetic fields ($\boldsymbol{E}_1$ and $\boldsymbol{B}_1$) interact to produce a net transport of electromagnetic energy radially through surface A. To our knowledge, this quantity has not been measured in previous experiments, nor has it received extensive attention in theoretical or computational works. Tsui (1988) develops a theoretical treatment that highlights S_f as a channel for energy transport in an RFP plasma with a perfectly conducting shell, though the work includes no estimate or measurement of the relative size of this effect. Sovinec (1995) examines the process using DEBS (Schnack *et al.* 1987) nonlinear MHD simulations of an RFP plasma with a close-fitting, perfectly conducting shell. In those simulations the outwardly directed S_f within the plasma reaches $\sim10\%$ of input power from the external supplies. The transported energy is deposited into resonant modes near the reversal surface, a key mechanism in sustainment of the dynamo process. With the perfectly conducting boundary in the DEBS simulation, no fluctuation-induced Poynting flux is observed at the extreme edge, as tangential electric field fluctuation amplitudes must vanish at the wall.

In this paper, we present measurements of magnetic tearing fluctuation-driven Poynting flux from an RFP experiment using an insertable probe, to our knowledge the first measurements of this quantity in a high-temperature magnetized plasma, and show that the flux plays a key role in the plasma's self-organization process. During sawtooth crash relaxation events, the outward flux corresponds to transient power levels much larger than the input power and comparable to the global equilibrium magnetic energy loss rate. The time-average flux is observed to reach a maximum at the magnetic reversal surface, where it corresponds to $\sim65\%$ of the input power. At the extreme edge the time-average flux corresponds to $\sim20\%$ of the input, impossible under the assumption of a perfectly conducting plasma boundary but evidently made possible in the experiment by a resistive layer at the boundary. We develop a simple model of a cylindrical, incompressible, resistive-MHD plasma with resistive boundary, which predicts that the fluctuation-induced Poynting flux out of the plasma edge corresponds approximately to the power lost from

the equilibrium magnetic field due to the dynamo EMF. The probe measurements of this flux are roughly as predicted by the model upon substitution of time-resolved cylindrical equilibrium measurement data from the experiment.

2. Model

To examine electromagnetic power balance in an RFP, we develop a simple Poynting's theorem model for an incompressible, resistive-MHD plasma with cylindrical flux surfaces and a resistive boundary. We write each quantity (such as pressure) as $p = p_0 + p_1$, the sum of mean (flux-surface average or equilibrium) and fluctuating parts, respectively, where $\langle p \rangle = p_0$ and $\langle p_1 \rangle = 0$. We define the flux-surface average of a vector quantity (Moffatt 1978; Krause & Rädler 1980; Tsui 1988; Ji *et al.* 1994; Ji 1999) as the vector sum of the flux-surface averages of its scalar components (Rädler 2007) in cylindrical coordinates. For example, the average current density $\boldsymbol{J}$ is written $\langle \boldsymbol{J} \rangle = \langle J_r \rangle \hat{\boldsymbol{r}} + \langle J_\phi \rangle \hat{\boldsymbol{\phi}} + \langle J_z \rangle \hat{\boldsymbol{z}}$. Note that the key results of this section can also be found by an alternative treatment using only flux-surface averages of scalars. The flux-surface average of a product of a single fluctuating quantity and a mean quantity is zero (e.g. $\langle \boldsymbol{v}_1 \times \boldsymbol{B}_0 \rangle = 0$), while the average of a product of two or more fluctuating quantities can be non-zero (e.g. $\langle \boldsymbol{v}_1 \times \boldsymbol{B}_1 \rangle$).

We begin by stating Poynting's theorem

$$\frac{1}{\mu_0} \int (\boldsymbol{E} \times \boldsymbol{B}) \cdot \mathrm{d}\boldsymbol{A} + \frac{1}{\mu_0} \int \boldsymbol{B} \cdot \dot{\boldsymbol{B}} \, \mathrm{d}V + \int \boldsymbol{E} \cdot \boldsymbol{J} \, \mathrm{d}V = 0, \qquad (2.1)$$

which represents the balance between the Poynting flux through a surface, the change of magnetic energy in the volume contained by the surface, and volumetric power transfer, which includes Ohmic dissipation. Assuming a fluid velocity $\boldsymbol{v}$ with no mean part and a non-fluctuating resistivity η for simplicity, Ohm's law is given by

$$\boldsymbol{E} + \boldsymbol{v}_1 \times \boldsymbol{B} = \eta \boldsymbol{J}, \qquad (2.2)$$

where the flux-surface average of the second term is the dynamo EMF, $\langle \boldsymbol{v}_1 \times \boldsymbol{B}_1 \rangle$, and the fluctuating part is $\boldsymbol{v}_1 \times \boldsymbol{B}_0 + \boldsymbol{v}_1 \times \boldsymbol{B}_1 - \langle \boldsymbol{v}_1 \times \boldsymbol{B}_1 \rangle$. Since Maxwell's equations are linear, Poynting's theorem (2.1) holds separately for the mean and fluctuating parts of the electromagnetic quantities. Substitution of the electric fields from the respective Ohm's laws (2.2) into the power transfer terms provides results that are then flux-surface averaged, becoming

$$\frac{1}{\mu_0} \int (\boldsymbol{E}_0 \times \boldsymbol{B}_0) \cdot \mathrm{d}\boldsymbol{A} + \frac{1}{\mu_0} \int \boldsymbol{B}_0 \cdot \dot{\boldsymbol{B}}_0 \, \mathrm{d}V + \int \eta J_0^2 \, \mathrm{d}V - \int \langle \boldsymbol{v}_1 \times \boldsymbol{B}_1 \rangle \cdot \boldsymbol{J}_0 \, \mathrm{d}V = 0 \qquad (2.3)$$

and

$$\frac{1}{\mu_0} \int \langle \boldsymbol{E}_1 \times \boldsymbol{B}_1 \rangle \cdot \mathrm{d}\boldsymbol{A} + \frac{1}{\mu_0} \int \langle \boldsymbol{B}_1 \cdot \dot{\boldsymbol{B}}_1 \rangle \, \mathrm{d}V + \int \eta \langle J_1^2 \rangle \, \mathrm{d}V$$
$$- \int \langle \boldsymbol{v}_1 \times \boldsymbol{B}_0 \cdot \boldsymbol{J}_1 \rangle \, \mathrm{d}V - \int \langle \boldsymbol{v}_1 \times \boldsymbol{B}_1 \cdot \boldsymbol{J}_1 \rangle \, \mathrm{d}V = 0. \qquad (2.4)$$

Note that the product $\langle \boldsymbol{v}_1 \times \boldsymbol{B}_1 \rangle \cdot \boldsymbol{J}_1$ averages to zero and so does not appear in (2.4). These two equations can be added together to yield the flux-surface average of Poynting's

theorem for the total electromagnetic quantities,

$$\frac{1}{\mu_0} \int \langle \boldsymbol{E} \times \boldsymbol{B} \rangle \cdot \mathrm{d}\boldsymbol{A} + \frac{1}{\mu_0} \int \langle \boldsymbol{B} \cdot \dot{\boldsymbol{B}} \rangle \, \mathrm{d}V + \int \eta \langle J^2 \rangle \, \mathrm{d}V - \int \langle \boldsymbol{v}_1 \times \boldsymbol{B} \cdot \boldsymbol{J} \rangle \, \mathrm{d}V = 0, \quad (2.5)$$

remembering that flux-surface averages of a product of one mean and one fluctuating quantity equals zero (e.g. $\langle \boldsymbol{E}_0 \times \boldsymbol{B}_1 \rangle = 0$). The expansion

$$-\langle \boldsymbol{v}_1 \times \boldsymbol{B} \cdot \boldsymbol{J} \rangle = -\langle \boldsymbol{v}_1 \times \boldsymbol{B}_1 \cdot \boldsymbol{J}_0 \rangle - \langle \boldsymbol{v}_1 \times \boldsymbol{B}_0 \cdot \boldsymbol{J}_1 \rangle - \langle \boldsymbol{v}_1 \times \boldsymbol{B}_1 \cdot \boldsymbol{J}_1 \rangle - \langle \boldsymbol{v}_1 \times \boldsymbol{B}_0 \cdot \boldsymbol{J}_0 \rangle$$

$$= -\langle \boldsymbol{v}_1 \times \boldsymbol{B}_1 \cdot \boldsymbol{J}_0 \rangle - \langle \boldsymbol{v}_1 \times \boldsymbol{B}_0 \cdot \boldsymbol{J}_1 \rangle - \langle \boldsymbol{v}_1 \times \boldsymbol{B}_1 \cdot \boldsymbol{J}_1 \rangle \quad (2.6)$$

was also used. Note that (2.5) can also be derived directly from (2.1) by substituting (2.2) into the power transfer term and then flux-surface averaging. Assuming that the fluctuation evolves slowly compared with an Alfvén time, which is true of tearing modes in typical experiments (Ortolani & Schnack 1993), the fluctuation is considered to be approximately in equilibrium. If we further assume that flows are slow compared with the sound speed, which is consistent with RFP observations (Fontana *et al.* 2000), we neglect contributions of flow and viscous dissipation and treat the equilibrium as magnetostatic. Under these assumptions,

$$-\langle (\boldsymbol{v}_1 \times \boldsymbol{B}) \cdot \boldsymbol{J} \rangle = \langle \boldsymbol{v}_1 \cdot \boldsymbol{\nabla} p_1 \rangle. \quad (2.7)$$

The proof for (2.7) follows. Since $p_1 = p - \langle p \rangle$, we have

$$\boldsymbol{\nabla} p_1 = \boldsymbol{\nabla} p - \boldsymbol{\nabla} \langle p \rangle = \boldsymbol{\nabla} p - \langle \boldsymbol{\nabla} p \rangle, \quad (2.8)$$

where the second equality follows from the definition of a flux-surface average of a vector (Rädler 2007). With a magnetostatic equilibrium, this can be rewritten as

$$\boldsymbol{\nabla} p_1 = \boldsymbol{J} \times \boldsymbol{B} - \langle \boldsymbol{J} \times \boldsymbol{B} \rangle = \boldsymbol{J}_0 \times \boldsymbol{B}_1 + \boldsymbol{J}_1 \times \boldsymbol{B}_0 + \boldsymbol{J}_1 \times \boldsymbol{B}_1 - \langle \boldsymbol{J}_1 \times \boldsymbol{B}_1 \rangle, \quad (2.9)$$

where each term that is the flux-surface average of a product including a single fluctuating quantity equals zero and is neglected. Dotting this with $\boldsymbol{v}_1$ and flux-surface averaging the result gives

$$\langle \boldsymbol{v}_1 \cdot \boldsymbol{\nabla} p_1 \rangle = \langle \boldsymbol{v}_1 \cdot (\boldsymbol{J}_0 \times \boldsymbol{B}_1) \rangle + \langle \boldsymbol{v}_1 \cdot (\boldsymbol{J}_1 \times \boldsymbol{B}_0) \rangle + \langle \boldsymbol{v}_1 \cdot (\boldsymbol{J}_1 \times \boldsymbol{B}_1) \rangle \quad (2.10)$$

where we have recognized that $\langle \boldsymbol{v}_1 \cdot \langle \boldsymbol{J}_1 \times \boldsymbol{B}_1 \rangle \rangle = 0$. If we expand the final integrand in (2.5) and use vector identities, we find that

$$-\langle \boldsymbol{v}_1 \times \boldsymbol{B} \cdot \boldsymbol{J} \rangle = \langle \boldsymbol{v}_1 \cdot \boldsymbol{J}_0 \times \boldsymbol{B}_1 \rangle + \langle \boldsymbol{v}_1 \cdot \boldsymbol{J}_1 \times \boldsymbol{B}_0 \rangle + \langle \boldsymbol{v}_1 \cdot \boldsymbol{J}_1 \times \boldsymbol{B}_1 \rangle = \langle \boldsymbol{v}_1 \cdot \boldsymbol{\nabla} p_1 \rangle \quad (2.11)$$

as needed. Inserting (2.7) into (2.5), the flux-surface averaged Poynting's theorem becomes

$$\frac{1}{\mu_0} \int \langle \boldsymbol{E} \times \boldsymbol{B} \rangle \cdot \mathrm{d}\boldsymbol{A} + \frac{1}{\mu_0} \int \langle \boldsymbol{B} \cdot \dot{\boldsymbol{B}} \rangle \, \mathrm{d}V + \int \eta \langle J^2 \rangle \, \mathrm{d}V + \int \langle \boldsymbol{v}_1 \cdot \boldsymbol{\nabla} p_1 \rangle \, \mathrm{d}V = 0. \quad (2.12)$$

Since the ϕ, z integrations in the flux-surface average are the same integration variables as are present in the volume integral, the flux-surface average can be brought outside of the last volume integral on the left. Assuming that flows are incompressible ($\boldsymbol{\nabla} \cdot \boldsymbol{v}_1 = 0$), the last volume integral in (2.12) can be rewritten as a surface integral so that

$$\frac{1}{\mu_0} \int \langle \boldsymbol{E} \times \boldsymbol{B} \rangle \cdot \mathrm{d}\boldsymbol{A} + \frac{1}{\mu_0} \int \langle \boldsymbol{B} \cdot \dot{\boldsymbol{B}} \rangle \, \mathrm{d}V + \int \eta \langle J^2 \rangle \, \mathrm{d}V + \left\langle \int p_1 \boldsymbol{v}_1 \cdot \mathrm{d}\boldsymbol{A} \right\rangle = 0, \quad (2.13)$$

where the last integral corresponds to volumetric contributions to the power balance due to flow fluctuations, including the dynamo EMF. If this expression is examined at the plasma

edge where $p_1 = 0$ holds, the last integral vanishes. For this case, we separate quantities into mean and fluctuating parts, giving

$$
\overbrace{\frac{1}{\mu_0} \int (\boldsymbol{E}_0 \times \boldsymbol{B}_0) \cdot \mathrm{d}\boldsymbol{A}}^{S_0} + \overbrace{\int_{\text{total}} \eta J_0^2 \, \mathrm{d}V}^{P_{\text{ohm}}} + \overbrace{\frac{1}{\mu_0} \int_{\text{total}} \boldsymbol{B}_0 \cdot \dot{\boldsymbol{B}}_0 \, \mathrm{d}V}^{P_{\text{mag},0}}
$$

$$
+ \underbrace{\frac{1}{\mu_0} \int_{\text{total}} \langle \boldsymbol{B}_1 \cdot \dot{\boldsymbol{B}}_1 \rangle \mathrm{d}V}_{P_{\text{mag},1}} + \underbrace{\frac{1}{\mu_0} \int \langle \boldsymbol{E}_1 \times \boldsymbol{B}_1 \rangle \cdot \mathrm{d}\boldsymbol{A}}_{S_f} = 0, \tag{2.14}
$$

where we have also assumed that the $\eta \langle J_1^2 \rangle$ integral of Ohmic losses due to fluctuations is negligible compared with any of the other integrals. Variable names have been assigned to each term for easy reference. This equation shows the expected global power balance between terms representing the inwardly directed equilibrium Poynting flux provided by the external power supplies through the plasma's surface (S_0), the equilibrium Ohmic loss rate in the plasma volume (P_{ohm}), the change of magnetic energy (both in the mean field $P_{\text{mag},0}$ and fluctuations $P_{\text{mag},1}$) and the fluctuation-induced Poynting flux S_f. Note that the assumption of a resistive plasma boundary rather than a perfectly conducting boundary permits a non-zero tangential E_1 and therefore a non-zero S_f.

3. Experiments

Experiments were conducted in the Madison Symmetric Torus (MST) (Dexter *et al.* 1991), a medium-sized RFP with major radius $R = 1.5$ m and minor radius $a = 0.52$ m. The plasma is surrounded by a thick, close-fitting conducting shell, and a toroidal rail limiter at the midplane extending ~ 1 cm into the plasma determines the plasma–vacuum boundary. Time-resolved global measurements include plasma current, toroidal-field shell current, external flux loops from which are derived loop voltages and magnetic fluxes, and an edge toroidal array for mode decomposition of magnetic fluctuations. Time-resolved electron temperature profiles were obtained with Thomson scattering (Parke *et al.* 2012).

To measure S_f, a probe was inserted into the edge region of low-current ($I_\text{p} \approx 205$ kA) plasmas with 20.5 V loop voltage and input power $S_0 \sim 4.2$ MW. Central chord-average electron density is $n_e \approx 1 \times 10^{13}$ cm^{-3}, while the edge region of radii r sampled by the probe ($0.77 < r/a < 1.0$, where $r/a = 0.85$ is the magnetic reversal surface location) has $n_e \sim (1–5) \times 10^{12}$ cm^{-3}, temperatures $T_e \sim T_i \leqslant 50$ eV and volume-average mean magnetic field $|\boldsymbol{B}_0| \approx 1100$ G. The plasma current and insertion depths were chosen to ensure probe survival and negligible plasma perturbation.

The insertable probe (Thuecks *et al.* 2017) was constructed to allow measurement of poloidal and toroidal electric and magnetic field fluctuations simultaneously and in close spatial proximity so that the radial S_f can be determined. Eight electrodes were spaced evenly (0.59 cm spacing) on the edges of a radially facing square and were used to measure the floating potential V_f. Electric field components in the poloidal (toroidal) direction were approximated using $E \approx -(V_{f2} - V_{f1})/(x_2 - x_1)$ where electrodes are separated poloidally (toroidally) by a distance $x_2 - x_1$. Here, we assumed small gradients in the electron temperature fluctuations, justified by previous comparisons of independent electrostatic measurements (Stone 2013), allowing us to approximate the fluctuating electric field using the floating potentials rather than plasma potentials. The inductive part of the fluctuating electric field is expected to be negligibly small in the present context (Ji *et al.* 1996; Bonfiglio, Cappello & Escande 2005).
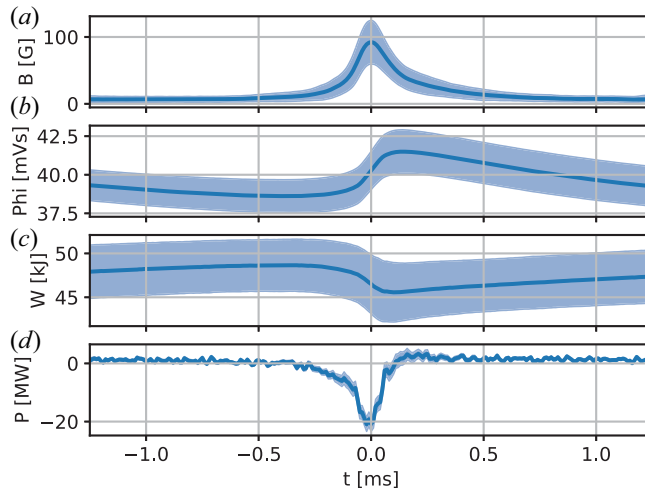
FIGURE 1. Time-resolved ensembled experimental data showing sawtooth crash event at $t = 0$: (*a*) amplitude of toroidal component of magnetic fluctuation with toroidal mode number $n = 1$, dominant at edge; (*b*) equilibrium toroidal flux; (*c*) equilibrium magnetic energy from cylindrical equilibrium fitting; (*d*) rate of change of equilibrium magnetic energy.

Magnetic fields were measured using an internal B-dot cube located along the radial axis 0.51 cm below the probe's electrode plane. Using this cube, $\dot{\boldsymbol{B}}$ can be measured in three orthogonal directions. The $\dot{\boldsymbol{B}}$ signal from the B-dot cube was differentially amplified and was then numerically integrated during analysis to find $\boldsymbol{B}$. Analysed data was taken during the plasma current flattop when plasma conditions remained relatively stationary.

Measured quantities are examined with respect to the quasiperiodic sawtooth cycle, with datasets from (typically) hundreds of sawteeth in many shots sliced into short time series centred around the sawtooth crashes for ensemble analysis. The fluctuating part of these quantities is then found by calculating the average time-resolved signal over many sawteeth and subtracting it from the individual sawtooth datasets.

Natural plasma rotation makes a time-resolved ensemble average for a fluctuating quantity an approximate spatial average over an equilibrium magnetic flux surface. The probe is traversed by a randomly phased extent of a rotating flux surface in each sawtooth dataset. Thus, by averaging over many sawtooth datasets we approximate a time-resolved flux-surface average. The duration of the ensemble time windows matches the typical sawtooth period, so the time average of an ensemble-averaged quantity over the window reflects its sawtooth cycle average.

4. Results

Quasiperiodic sawtooth crash magnetic relaxation events punctuate the plasma current flattop. Key plasma quantities time-resolved over a sawtooth ensemble are shown in figure 1. Figure 1(*a*) shows the amplitude of the toroidal component of magnetic fluctuations with toroidal mode number $n = 1$, dominant at the edge and measured by an edge toroidal array. During the crash, these tearing magnetic fluctuations peak in amplitude, equilibrium toroidal flux (figure 1*b*) is generated, and equilibrium magnetic energy is lost (figure 1*c*,*d*) in magnetic relaxation. The magnitude of the loss rate of equilibrium magnetic energy peaks at ∼20 MW during the crash, which is several times the input power.
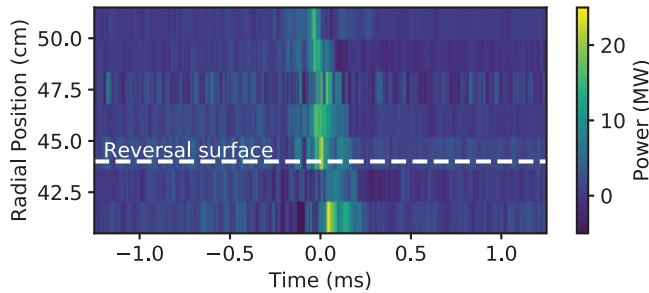
FIGURE 2. Surface-integrated outwardly directed Poynting flux due to fluctuations versus time, measured for the experimental range of inserted probe radii in the plasma edge region. Measurement uncertainties are a few MW during the crash and around 1 MW far from the crash.

Large-scale tearing modes energized at the sawtooth crash drive a nonlinear cascade supporting broadband fluctuations of electric and magnetic fields (Rempel *et al.* 1991, 1992; Sarff *et al.* 1993; Ren *et al.* 2011; Thuecks *et al.* 2017), which interact to drive the outwardly directed Poynting flux S_f that we measure with the probe. Almost all of this flux is due to the interaction of low-frequency fluctuations associated with large-scale tearing modes (as opposed to high-frequency, small-scale fluctuations which are also observed). Figure 2 shows sawtooth-averaged measurements of S_f for the experimental range of inserted probe radii versus time relative to the sawtooth crash relaxation event. The measured S_f peaks sharply in time at the crash, reaching values of $\sim$20–25 MW, several times the input power, for most of the probe locations including the outermost edge channels, with a significantly smaller peak just inside the reversal surface. There is the hint of a trend in the radial variation of the times of S_f peaks, but its significance is unclear given the measurement uncertainties of several MW during the crash. Measured fluxes at times far from the crash are relatively very small.

Time averages of S_f (over the sawtooth cycles shown in figure 2) for each probe radial location are plotted in figure 3. The time-average outward flux reaches $\sim$2.8 MW, or $\sim$65 % of the input power, both near the reversal surface at $r \approx 44$ cm and at the deepest probe location of $r = 40.5$ cm. It is significantly smaller just inside the reversal surface. We characterize the flux leaving the plasma using the $r = 49.5$ cm probe location, finding a time average value of $\sim$0.8 MW, or $\sim$20 % of the input power. This location may be close enough to the wall for the S_f measurement to be affected by the probe port equilibrium magnetic field error (Fimognari *et al.* 2010), though the measured values are similar to those at $r = 47.5$ cm, not likely to be strongly affected by the port.

This $r = 49.5$ cm ($r/a = 0.95$) edge probe measurement is compared with the prediction of the MHD model discussed above by first evaluating the terms other than S_f in (2.14), as shown in figure 4. In figure 4(*a*), the negative Poynting flux integral $S_0 = \mu_0^{-1} \int \boldsymbol{E}_0 \times \boldsymbol{B}_0 \cdot d\boldsymbol{A}$ represents the inwardly directed power provided by the external supplies. This is the sum of the surface loop voltage times the circuit current for the Ohmic and the toroidal magnetic field supplies. It is dominated by the steady input from the Ohmic supply, though a small transient feature indicating some power back into the toroidal supply is evident around $t = 0$. The volume integrals in this comparison representing Ohmic losses $P_{\mathrm{Ohm}} = \int \eta J_0^2 \, dV$ and power to equilibrium magnetic fields $P_{\mathrm{mag},0} = \mu_0^{-1} \int \boldsymbol{B}_0 \cdot \dot{\boldsymbol{B}}_0 \, dV$ are derived by fitting equilibrium magnetics data to a cylindrical 'alpha' model (Antoni *et al.* 1986), a well-established and accurate approximation for self-organizing RFPs. At each time point, the RFP magnetic equilibrium
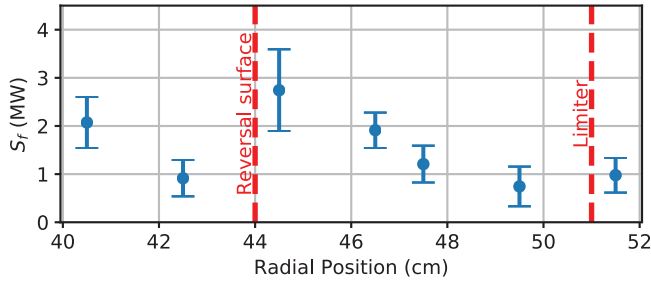
FIGURE 3. Time averages of surface-integrated outwardly directed Poynting flux due to fluctuations, measured for the experimental range of inserted probe radial locations in the plasma edge.

profiles in those integrals are available given the edge equilibrium poloidal and toroidal magnetic fields and equilibrium toroidal flux. Here P_{Ohm} includes Thomson scattering data of electron temperature T fit for each time point to a parabolic profile, which is an adequate approximation over the sawtooth cycle. This provides a time-resolved Spitzer resistivity profile $\eta \sim T^{-3/2}$ which is scaled by a single constant multiplying factor so that $S_0 + P_{\text{Ohm}} + P_{\text{mag},0} = 0$ holds on time average far from sawtooth crash events, i.e. when fluctuations are small. A rough estimate of the global power to fluctuating magnetic fields $P_{\text{mag},1} = \mu_0^{-1} \int \langle \boldsymbol{B}_1 \cdot \dot{\boldsymbol{B}}_1 \rangle \, \mathrm{d}V$ is calculated by assuming uniform fluctuations throughout the plasma volume equal to those measured at the edge. Though the fluctuation amplitudes actually have a radial profile, this simplifying approximation is broadly compatible with available nonlinear MHD simulations of RFPs. It can be heuristically motivated by the understanding that the dominant mode experimentally detected at the edge is the edge-resonant $n = 1$ mode, whose profile is peaked near the edge and can be expected to be similar in peak amplitude to core-resonant modes. The estimate is small compared with $P_{\text{mag},0}$ during the crash.

In figure 4(*b*), the negative sum of these terms (labelled as 'MHD model') is shown to be roughly consistent with our probe measurement of S_f at $r = 49.5$ cm, though a discrepancy exists for a short time interval around the sawtooth crash. There is a short period of time immediately following the sawtooth crash during which S_f is observed to be negative, indicating inward energy transport, though the statistical significance of this feature is questionable. As in our simple MHD model of an incompressible plasma with a resistive edge, the large equilibrium magnetic field power loss rate during the sawtooth crash can be largely identified with tearing fluctuation-induced Poynting flux measured in the plasma edge.

5. Discussion

The fluctuation-induced Poynting flux is a key mechanism supporting magnetic relaxation in this self-organizing RFP plasma. Our experiments showing a finite measured value of the flux S_f at the edge indicate that it transports more than enough power through the plasma to energize the dynamo EMF driving the relaxation. As discussed in relation to figure 2, the measured S_f reaches instantaneous values of ∼25 MW in the edge region, comparable to the measured equilibrium loss rate $P_{\text{mag},0}$ and much larger than the input power S_0. In its radial profile, S_f is observed to drop from a higher value to a significantly lower value just inside the reversal surface and then to rise to a higher value just outside it. Hypothetically, the inside drop might correspond to power absorption into edge-resonant
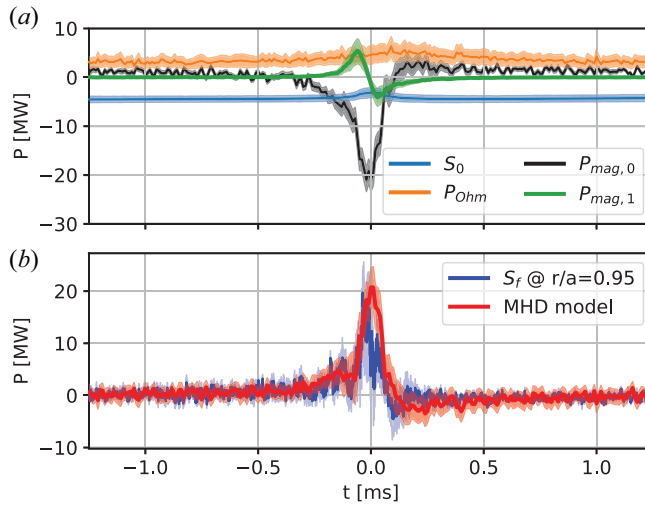
FIGURE 4. Time-resolved experimental quantities in global electromagnetic power balance: (*a*) with same signs as integrals in (2.14), the input power S_0 (blue), Ohmic losses P_{Ohm} (orange), power into equilibrium magnetic field $P_{\mathrm{mag},0}$ (black), estimated power into fluctuating magnetic field $P_{\mathrm{mag},1}$ (green); (*b*) probe-measured S_f (blue) and negative sum of terms in panel (*a*) (red).

fluctuations generating the dynamo EMF, which would also radiate power (originating in the equilibrium) corresponding to the rise just outside.

Considering (2.3), recognition that the experimentally measured S_0 and P_{Ohm} in figure 4(*a*) nearly balance each other during relaxation implies

$$P_{\mathrm{mag},0} \approx \int \langle \boldsymbol{v}_1 \times \boldsymbol{B}_1 \rangle \cdot \boldsymbol{J}_0 \, \mathrm{d}V, \qquad (5.1)$$

i.e. that the rapid loss of equilibrium energy during the crash in the experiment can be ascribed to dynamo EMF drive and antidrive of the equilibrium current, wherever they occur in the plasma. More comprehensively, subtracting (2.3) from (2.14) gives

$$\int \langle \boldsymbol{v}_1 \times \boldsymbol{B}_1 \rangle \cdot \boldsymbol{J}_0 \, \mathrm{d}V + S_f + P_{\mathrm{mag},1} \approx 0, \qquad (5.2)$$

which, considering figure 4(*b*), indicates that much of this same energy loss is transmitted to the edge and released from the plasma, with the remainder evidently available to power magnetic fluctuations during the crash. Furthermore, since $P_{\mathrm{mag},1}$ vanishes on time average, (5.2) suggests that almost all of the energy lost from the equilibrium field during the relaxation event leaves the plasma over time as S_f (apart from small fluctuation Ohmic losses). This picture is distinct from corresponding theoretical results such as Bhattacharjee & Hameiri (1986) involving perfectly conducting boundaries. Although the thick MST shell is highly conductive, the plasma boundary region, which we consider as including the extreme edge and the limiter, appears to behave resistively in the present context.

Ion heating by magnetic reconnection during relaxation, which accounts for approximately 15 %–20 % of the equilibrium field energy lost during the crash (Fiksel *et al.* 2009), is not included in our MHD analysis. This heating, which occurs most intensely during the sawtooth crash, may help to explain the discrepancy visible in

figure 4(*b*). Integration of the curves in figure 4(*b*) reveals that the energy carried out of the plasma by S_f during the sawtooth event represents $\sim$70 % of the MHD model prediction. When combined with ion heating estimates, 85 %–90 % of the energy is accounted for, with the remaining difference within measurement and model uncertainties.

The role played by S_f in the RFP's magnetic relaxation process highlights the importance of geometry and boundary conditions in self-organizing systems. As motivated by the form of Poynting's theorem and the discussion of Sovinec (1995) in the RFP context, electromagnetic energy must travel spatially across a system in order to be exchanged between multiple, nonlinearly coupled fluctuations and equilibrium. That the magnitude of this flux is apparently coupled to boundary conditions is indicated by comparing our experimental results with the nonlinear resistive-MHD simulations of Sovinec (1995). With the conducting boundary in the simulations, S_f identically vanishes in the extreme edge and, aside from Ohmic fluctuation losses, is evidently just sufficient within the plasma to drive the dynamo EMF, peaking radially at a time average of $\sim$10 % of the input power. In our experiments, the relaxation process seems to be much less efficient. The S_f in the edge region peaks at an instantaneous value of several times the input power and averages $\sim$65 % of it over time. The resistive character of the plasma boundary region allows an appreciable fraction to escape at the edge, $\sim$20 % of the input on average.

How the observed Poynting flux at the plasma edge is dissipated in the experiment is not clear. Some power might be lost directly onto the limiter, and some might be deposited into neutrals via charge exchange processes, followed by their loss to the wall. A related question is how the observed electromagnetic energy transport and loss at the plasma edge relates to global thermal energy balance. Formally, Poynting flux is closely related to the plasma E-cross-B flow, and thus S_f at the edge could correspond to the global loss of thermal plasma energy.

Future work will include deeper probe measurements of fluctuation-induced Poynting flux S_f to better determine the global character of this key transport mechanism. This could be combined with an equilibrium scan of the radial location of the RFP reversal surface, in particular to study the implied efficiency of the power transfer from equilibrium to dynamo EMF. We also intend to investigate direct correlations between S_f and the dynamo EMF as well as magnetic helicity using probes (Ji *et al.* 1994; Ji 1999; Stone 2013). Investigating detailed temporal correlations between such probe measurements and individual resonant mode activity may also help illuminate the role of S_f in the relaxation process. A new probe might be designed to internally measure the radial component of the $\langle p_1 \boldsymbol{v}_1 \rangle$ term in (2.13) relating to the volume integral of total dynamo-induced magnetic energy loss rate. New nonlinear MHD simulations of the RFP with explicitly resistive boundary conditions may provide further insight into the issues discussed in this work. More generally, the role of fluctuation-induced Poynting flux should be explored in other magnetized plasma systems, in particular those involving phenomena such as magnetic tearing, turbulence, relaxation or self-organization.

Funding

This work was supported by the United States Department of Energy, Office of Science, Office of Fusion Energy Sciences (grant numbers DE-FC02-05ER54814, DE-SC0018266).

Declaration of interests

The authors report no conflict of interest.

Data availability statement

The data that support the findings of this study are openly available in Zenodo at https://doi.org/10.5281/zenodo.4595818.

REFERENCES

ANTONI, V., MERLIN, D., ORTOLANI, S. & PACCAGNELLA, R. 1986 MHD stability analysis of force-free reversed field pinch configurations. *Nucl. Fusion* **26** (12), 1711–1717.

BHATTACHARJEE, A. & HAMEIRI, E. 1986 Self-consistent dynamolike activity in turbulent plasmas. *Phys. Rev. Lett.* **57** (2), 206–209.

BIEWER, T., FOREST, C., ANDERSON, J., FIKSEL, G., HUDSON, B., PRAGER, S., SARFF, J., WRIGHT, J., BROWER, D., DING, W., *et al.* 2003 Electron heat transport measured in a stochastic magnetic field. *Phys. Rev. Lett.* **91** (4), 045004.

BONFIGLIO, D., CAPPELLO, S. & ESCANDE, D.F. 2005 Dominant electrostatic nature of the reversed field pinch dynamo. *Phys. Rev. Lett.* **94**, 145001.

BRUNSELL, P.R., MAEJIMA, Y., YAGI, Y., HIRANO, Y. & SHIMADA, T. 1994 Edge plasma fluctuations and transport in a reversed-field pinch. *Phys. Plasmas* **1**, 2297–2307.

DEN HARTOG, D.J., CHAPMAN, J.T., CRAIG, D., FIKSEL, G., FONTANA, P.W., PRAGER, S.C. & SARFF, J.S. 1999 Measurement of core velocity fluctuations and the dynamo in a reversed-field pinch. *Phys. Plasmas* **6**, 1813–1821.

DEXTER, R.N., KERST, D.W., LOVELL, T.W., PRAGER, S.C. & SPROTT, J.C. 1991 The madison symmetric torus. *Fusion Technol.* **19**, 131.

FIKSEL, G., ALMAGRI, A.F., CHAPMAN, B.E., MIRNOV, V.V., REN, Y., SARFF, J.S. & TERRY, P.W. 2009 Mass-dependent ion heating during magnetic reconnection in a laboratory plasma. *Phys. Rev. Lett.* **103** (14), 145002.

FIKSEL, G., BENGTSON, R.D., CEKIC, M., DEN HARTOG, D., PRAGER, S.C., PRIBYL, P., SARFF, J., SOVINEC, C., STONEKING, M.R., TAYLOR, R.J., *et al.* 1996 Measurement of magnetic fluctuation-induced heat transport in tokamaks and RFP. *Plasma Phys. Control. Fusion* **38**, A213–A225.

FIMOGNARI, P.J., ALMAGRI, A.F., ANDERSON, J.K., DEMERS, D.R., SARFF, J.S., TANGRI, V. & WAKSMAN, J. 2010 Port hole perturbations to the magnetic field in MST. *Plasma Phys. Control. Fusion* **52**, 095002.

FONTANA, P.W., DEN HARTOG, D.J., FIKSEL, G. & PRAGER, S.C. 2000 Spectroscopic observation of fluctuation-induced dynamo in the edge of the reversed-field pinch. *Phys. Rev. Lett.* **85** (3), 566–569.

HO, Y.L. & CRADDOCK, G.G. 1991 Nonlinear dynamics of field maintenance and quasiperiodic relaxation in reversed-field pinches. *Phys. Fluids* B **3** (3), 721–734.

JI, H. 1999 Turbulent dynamos and magnetic helicity. *Phys. Rev. Lett.* **83**, 3198–3201.

JI, H., ALMAGRI, A.F., PRAGER, S.C. & SARFF, J.S. 1994 Time-resolved observation of discrete and continuous magnetohydrodynamic dynamo in the reversed-field pinch edge. *Phys. Rev. Lett.* **73**, 668–671.

JI, H., PRAGER, S.C., ALMAGRI, A.F., SARFF, J.S., YAGI, Y., HIRANO, Y., HATTORI, K. & TOYAMA, H. 1996 Measurement of the dynamo effect in a plasma. *Phys. Plasmas* **3**, 1935–1942.

KRAUSE, F. & RÄDLER, K.-H. 1980 *Mean-Field Magnetohydrodynamics and Dynamo Theory*. Akademie-Verlag.

KURITSYN, A., FIKSEL, G., ALMAGRI, A.F., BROWER, D.L., DING, W.X., MILLER, M.C., MIRNOV, V.V., PRAGER, S.C. & SARFF, J.S. 2009 Measurements of the momentum and current transport from tearing instability in the Madison Symmetric Torus reversed-field pinch. *Phys. Plasmas* **16** (5), 055903.

MARRELLI, L., MARTIN, P., PUIATTI, M.E., SARFF, J.S., CHAPMAN, B.E., DRAKE, J.R., ESCANDE, D.F. & MASAMUNE, S. 2021 The reversed field pinch. *Nucl. Fusion* **61**, 023001.

MOFFATT, H.K. 1978 *Magnetic Field Generation in Electrically Conducting Fluids*. Cambridge University Press.

NEBEL, R.A., CARAMANA, E.J. & SCHNACK, D.D. 1989 The role of $m = 0$ modal components in the reversed-field-pinch dynamo effect in the single fluid magnetohydrodynamics model. *Phys. Fluids* B **1** (8), 1671–1674.

ORTOLANI, S. & SCHNACK, D. 1993 *Magnetohydrodynamics of Plasma Relaxation*. World Scientific.

PARKE, E., HARTOG, D.J.D., MORTON, L.A., STEPHENS, H.D., KASTEN, C.P., REUSCH, J.A., HARRIS, W.H., BORCHARDT, M.T., FALKOWSKI, A.F., HURST, N.C., *et al.* 2012 Improvements to the calibration of the MST Thomson scattering diagnostic. *Rev. Sci. Instrum.* **83**, 10E324.

RÄDLER, K.-H. 2007 *Mean-Field Dynamo Theory: Early Ideas and Today's Problems*, pp. 55–72. Springer.

REMPEL, T.D., ALMAGRI, A.F., ASSADI, S., DEN HARTOG, D.J., HOKIN, S.A., PRAGER, S.C., SARFF, J.S., SHEN, W., SIDIKMAN, K.L., SPRAGINS, C.W., *et al.* 1992 Turbulent transport in the Madison Symmetric Torus reversed-field pinch. *Phys. Fluids* B **4**, 2136–2141.

REMPEL, T.D., SPRAGINS, C.W., PRAGER, S.C., ASSADI, S., DEN HARTOG, D.J. & HOKIN, S. 1991 Edge electrostatic fluctuations and transport in a reversed-field pinch. *Phys. Rev. Lett.* **67**, 1438–1441.

REN, Y., ALMAGRI, A.F., FIKSEL, G., PRAGER, S.C., SARFF, J.S. & TERRY, P.W. 2011 Experimental observation of anisotropic magnetic turbulence in a reversed field pinch plasma. *Phys. Rev. Lett.* **107** (19), 195002.

SARFF, J.S., ASSADI, S., ALMAGRI, A.F., CEKIC, M., DEN HARTOG, D.J., FIKSEL, G., HOKIN, S.A., JI, H., PRAGER, S.C., SHEN, W., *et al.* 1993 Nonlinear coupling of tearing fluctuations in the Madison Symmetric Torus. *Phys. Fluids* B **5**, 2540–2545.

SAUPPE, J.P. & SOVINEC, C.R. 2017 Extended MHD modeling of tearing-driven magnetic relaxation. *Phys. Plasmas* **24**, 056107.

SCHNACK, D.D., BARNES, D.C., MIKIC, Z., HARNED, D.S. & CARAMANA, E.J. 1987 Semi-implicit magnetohydrodynamic calculations. *J. Comput. Phys.* **70** (2), 330–354.

SERIANNI, G., MURARI, A., FIKSEL, G., ANTONI, V., BAGATIN, M., DESIDERI, D., MARTINES, E. & TRAMONTIN, L. 2001 Magnetic fluctuations and energy transport in RFX. *Plasma Phys. Control. Fusion* **43** (7), 919–927.

SOVINEC, C.R. 1995 Magnetohydrodynamic simulations of noninductive helicity injection in the reversed-field pinch and tokamak. PhD thesis, The University of Wisconsin–Madison.

STONE, D.R. 2013 Magnetic relaxation during oscillating field current drive in a reversed field pinch. PhD thesis, The University of Wisconsin–Madison.

TAYLOR, J.B. 1974 Relaxation of toroidal plasma and generation of reverse magnetic fields. *Phys. Rev. Lett.* **33**, 1139–1141.

THUECKS, D.J., ALMAGRI, A.F., SARFF, J.S. & TERRY, P.W. 2017 Evidence for drift waves in the turbulence of reversed field pinch plasmas. *Phys. Plasmas* **24** (2), 022309.

TSUI, H. 1988 Magnetic helicity transport and the reversed field pinch. *Nucl. Fusion* **28** (9), 1543–1554.